RSC Advances

PAPER

View Article Online
View Journal | View Issue

Cite this: *RSC Adv.*, 2021, **11**, 17431

Synthesis of luminescent thorium-based metal–organic frameworks with 1,2,4,5-tetrakis(4-carboxyphenyl)benzene†

Ting Yu, ‡[a] Zheng-hua Qian,[b] Lin Li,[bc] Xiao-ling Wu,[bc] Hui He,[a] Yan-bo Qiao[b] and Guo-an Ye*[a]

Received 5th March 2021
Accepted 16th April 2021

DOI: 10.1039/d1ra01742j

rsc.li/rsc-advances

Three new thorium-based MOFs based on 1,2,4,5-tetrakis(4-carboxyphenyl)benzene (H4TCPB) were obtained under a similar reaction system (metal salt, ligand, solvent, and acid are the same). Th(IV) forms the central unit of the MOFs in mononuclear and binuclear clusters, respectively. All the MOFs show blue ligand-based luminescence under an ultraviolet environment. This is the first time that multiple thorium-based MOFs with luminescence have been found with the same ligand.

1. Introduction

Metal–organic frameworks (MOFs), as functional materials with great potential, have been widely studied and applied in the fields of luminescence, adsorption, catalysis, and waste treatment since their discovery.[1,2] In recent years, with the gradual improvement of the study on transition metal elements and lanthanide-based MOFs, actinide-based MOFs have attracted wide attention and form a new research direction.[3] The 5f/6d/7s electron orbitals of actinides can easily be bonded by any element (the extranuclear electron configuration is $5f^{0-1}4}6d^{0-1}7s^{2}$), and they exhibit multiple oxidation states and have high coordination numbers. Therefore, actinides are more likely to react with ligands to form MOFs than transition metal elements and lanthanides. For example, uranyl-based MOFs with different topologies were synthesized using uranium(VI), and the properties of these compounds were characterized.[4–9]

As an important part of the actinide chemistry, thorium has attracted more attention with the development of the thorium uranium fuel cycle. Thorium exists stably in solution as Th(IV), which hydrolyzes and condenses in a solution to form oxygen-containing or hydroxy-containing clusters.[10] Compared with uranyl-based MOFs, the research progress of thorium-based MOFs is relatively slow.[11] Only a few Th – containing compounds in CCDC database are MOFs. Since O'Hare first cofounded a series of thorium-based MOFs (TOF-1, TOF-2, and TOF-3),[12–14] a number of constructed thorium-based MOFs have emerged newly, most of which are mononuclear, dimers, and trimers.[15–19] In recent years, some thorium-based MOFs similar to the octahedral hexagonal zirconium clusters of classical zirconium-based MOFs have been synthesized successively: Thierry *et al.* synthesized Th-UiO-66,[20] Li *et al.* synthesized Th-PCN-222,[21] Islamoglu *et al.* synthesized Th-MOF-808,[22] and Li *et al.* obtained a series of Th-UiO-66-X based on Th-UiO-66 by functional group modification.[23,24]

Unlike many of the photoluminescent uanyl-based MOFs found so far,[25,26] thorium does not have typical photoluminescence characteristic peaks, so these known thorium-based MOFs focus more on the adsorption properties of materials.[16,17,24] In this study, Th(IV) and 1,2,4,5-tetrad(4-carboxyl phenyl)benzene were used as raw materials for hydrothermal reaction. Three kinds of thorium-based MOFs with fluorescent properties were obtained without changing the reaction system except the reaction temperature, time, and regulator concentration. Like most known thorium-based MOFs, Th(IV) in our synthetic thorium-based MOFs exist as mononuclear and dinuclear clusters, respectively. These do not have hexagonal zirconium cluster structures similar to Zr-CAU-24.[27]

2. Experimental section

^{232}Th used in this study is a radioactive and chemically toxic nuclide with the daughter of radioactive Ra-228. Standard precautions for handling radioactive materials should be followed.

2.1 Materials and methods

$Th(NO_3)_4 \cdot 5H_2O$ (99.5%, Shanghai Aladdin Biochemical Technology Co., Ltd), 1,2,4,5-tetrakis(4-carboxyphenyl)benzene

[a]China Institute of Atomic Energy, Department of Radiochemistry, Beijing 102413, China. E-mail: yeguoan@ciae.ac.cn

[b]Shanghai Institute of Applied Physics, Chinese Academy of Sciences, Shanghai 201800, China

[c]University of Chinese Academy of Sciences, Beijing 100049, China

† Electronic supplementary information (ESI) available: PXRD patterns, SEM photographs, BET and pore-size distribution, TGA curves, IR spectra, emission and excitation spectra (PDF) and CIF files. CCDC 2067961–2067963. For ESI and crystallographic data in CIF or other electronic format see DOI: 10.1039/d1ra01742j

‡ Ungraduated students of Chinese Academy of Sciences.

(H4TCPB, 98%, Jilin Chinese Academy of Sciences-Yanshen Technology Co., Ltd), *N*,*N*′-dimethylformamide (DMF, 99.5%, Meryer Shanghai Chemical Technology Co., Ltd), trifluoroacetic acid (99%, Shanghai Macklin Biochemical Co., Ltd), ethanol (EtOH, 95%, Sinopharm Chemical Reagent Co., Ltd), *n*-hexane (97%, Meryer Shanghai Chemical Technology Co., Ltd), dichloromethane (DCM, 99.5%, Sinopharm Chemical Reagent Co., Ltd).

Compound 1. A mixture of $Th(NO_3)_4 \cdot 5H_2O$ (11.40 mg, 0.02 mmol), H4TCPB (11.17 mg, 0.02 mmol), DMF (1.5 mL), trifluoroacetic acid (0.025 mL) in a 7 mL capped vial was heated at 130 °C for 6 h and then cooled to room temperature. Colorless crystals were filtered, washed with EtOH, and dried at room temperature. Yield, 54.3% based on H4TCPB. Elemental analysis observed calcd for $Th(TCPB)(C_3H_7NO)_3(H_2O)_2$, $C_{43}H_{43}N_3ThO_{13}$, C, 49.54%; H, 4.13%; N, 4.03%. Found: C, 49.14%; H, 4.38%; N, 4.30%.

Compound 2. A mixture of $Th(NO_3)_4 \cdot 5H_2O$ (22.81 mg, 0.04 mmol), H4TCPB (11.17 mg, 0.02 mmol), DMF (3 mL), trifluoroacetic acid (0.5 mL) in a 10 mL Teflon-lined stainless steel autoclave. The autoclave was sealed and heated at 120 °C for 2 days. Pressure of the autoclave was relieved and reheated at 120 °C for 4 days, then cooled to room temperature. Pale yellow crystals were filtered, washed with EtOH, and dried at room temperature. Yield, 55.8% based on H4TCPB. Elemental analysis observed calcd for $Th_2O_3(TCPB)(H_2O)_4(C_3H_7NO)_6(H_2O)_3$, $C_{52}H_{74}N_6Th_2O_{24}$, C, 38.27%; H, 4.54%; N, 5.15%. Found: C, 38.27%; H, 4.36%; N, 5.25%.

Compound 3. A mixture of $Th(NO_3)_4 \cdot 5H_2O$ (11.40 mg, 0.02 mmol), H4TCPB (11.17 mg, 0.02 mmol), DMF (1.5 mL), trifluoroacetic acid (0.025 mL) in a 7 mL capped vial was heated at 80 °C for 2 days and then cooled to room temperature. Colorless crystals were filtered, washed with EtOH, and dried at room temperature. Yield, 43.8% based on H4TCPB. Elemental analysis observed calcd for $Th(TCPB)(C_3H_7NO)(H_2O)(C_3H_7NO)_2(H_2O)$, $C_{43}H_{43}N_3ThO_{13}$, C, 49.54%; H, 4.13%; N, 4.03%. Found: C, 49.42%; H, 4.16%; N, 4.28%.

The preparation of compound **2** was very accidental. A batch of samples was heated for 2 days, and no crystals were found when the autoclave was opened. Then the samples were heated for different times, and compound **2** was obtained in 4 days. We tried to heat the samples continuously for six days or more, but we didn't get the desired results. Therefore, cooling and pressure relief in the preparation process must be carried out.

Standard precautions were performed for handling radioactive materials during work with thorium-containing materials. The products were filtered and then dried in the air for analytical testing.

2.2 Single crystal X-ray diffraction (SCXRD)

Suitable crystals were selected and data collections were performed on a Bruker APEX-II CCD diffractometer equipped with a Turbo X-ray source (Ga Kα radiation, $\lambda = 1.34180$ Å) adopting the direct-drive rotating-anode technique and a CMOS detector. The crystal was kept at 169.98 K during data collection. Using Olex2,[28] the structure was solved with the ShelXT[29] structure solution program using intrinsic phasing and refined with the ShelXL[30] refinement package using least squares minimization. The contributions to scattering due to these highly disordered solvent molecules were removed using the SQUEEZE routine of PLATON. Crystallographic data of compound **1–3** are given in Table S1† and the selected bond lengths are presented in Table S2.†

2.3 Powder X-ray diffraction (PXRD)

The PXRD data were collected from 5° to 50° with a step of 0.02° on a Bruker D8 Advance diffractometer with Cu Kα radiation ($\lambda = 1.54178$ Å). The calculated PXRD pattern was produced from the CIFs using the SHELXTL-XPOW program. The phase purity of samples was confirmed by comparison of their simulated powder XRD patterns (Fig. S1†).

2.4 Scanning electron microscope morphology (SEM)

SEM images were recorded on a Zeiss Merlin Compact LEO 1530 VP scanning electron microscope. Three thorium-based MOFs crystals were shown in sheets (20–40 m), biconical pillars (40–80 m), and lumps (30–50 m) under microscope (200 times) (Fig. S2†).

2.5 Elemental analyses (EA)

The element content (C, H, and N) of the samples were performed with an Elementar Vario EL III.

2.6 Infrared spectroscopy (IR)

The IR spectra in the range of 400 cm^{-1} to 4000 cm^{-1} was recorded by a Thermo Nicolet 6700 FTIR spectrometer equipped with a diamond attenuated total reflectance (ATR) accessory.

2.7 Thermogravimetric analysis (TGA)

The TGA was carried out on a Mettler-Toledo TGA/DSC1 (N_2) with a heating rate of 10 °C min^{-1} from 30 °C to 900 °C.

2.8 Gamma irradiation

The prepared samples were irradiated by a 100 kCi radiation source (^{60}Co) at a dose of 20 kGy to 100 kGy.

2.9 Surface area measurement

The N_2 adsorption isotherms were recorded at 77 K by using a micromeritics ASAP 2020 surface area and a porosity analyzer. NLDFT method was used for calculation of pore size distribution. Before the adsorption measurements, compound **1–3** were soaked in *n*-hexane and DCM for 6 h to exchange DMF guest solvent, respectively. The samples were then loaded into quartz glass tubes and outgassed under dynamic vacuum (10^{-2} kPa) at 100 °C for 6 h.

2.10 Fluorescence spectroscopy

The photoluminescence emission spectra were performed on an Edinburgh Instrument FLS 980 fluorescence spectrometer.

3. Results and discussion

3.1 Crystal structures

Compound 1. SCXRD studies of compound **1** reveal that it crystallizes in the monoclinic space group *P*2/*n*. This crystal structure is constructed from the eight-coordinate Th(IV) units that are both bridged and chelated by the H4TCPB (Fig. 1a). The packing diagram of compound **1** indicates that the complex has two kinds of quadrilateral windows (5.82 Å × 8.87 Å and 5.08 Å × 9.35 Å diagonal distances) along [100] direction (Fig. 1b). The thorium atom is coordinated by eight carboxyl oxygen atoms from six distinct ligand molecules (Fig. 1c). The Th–O (carboxyl) bond lengths are in the range of 2.390(30)–2.524(29) Å. Both the metal cation and the ligand are 6-fold node (Fig. 1d).

Compound 2. SCXRD studies of compound **2** reveal that it crystallizes in the orthorhombic space group *Cmca*. This structure consists of a three-dimensional network constructed from the two ten-coordinate Th(IV) units that are chelated and bridged by H4TCPB (Fig. 2a). The packing diagram of compound **2** indicates two rhombic windows (1.40 Å × 10.89 Å and 4.58 Å × 11.20 Å diagonal distances) along [100] direction (Fig. 2b). The two thorium atoms form a centrally-symmetric binuclear cluster $Th_2O_3(H_2O)_4(CO_2)_2(CO)_4$ by relying on the Th–Th bond and Th–O–Th bond (Fig. 2C). The Th–Th distance is 3.9322(9) Å and the Th–O (Th) bond lengths are in the range of 2.327(7)–2.389(7) Å. The remaining coordination oxygen atoms of thorium come from 4 carboxyl groups and 2 coordination water molecules of 4 different ligand molecules with Th–O bond lengths ranging from 2.361(18) Å to 2.541(10) Å. Each dimer is thus an 8-fold node, whereas the ligand is a 6-fold node (Fig. 2d).

Compound 3. SCXRD studies of compound **3** reveal that it crystallizes in the monoclinic space group *P*21/*n*. This structure is constructed from the nine-coordinate Th(IV) units as shown in blue that are bridged by H4TCPB (Fig. 3a). The packing diagram of compound **3** indicates a dumbbell windows (1.15 Å × 27.37 Å) along [100] direction (Fig. 3b). The thorium atom is coordinated by carboxyl oxygen atoms (seven from six distinct ligand molecules and one from DMF molecule) and coordination water. Each ligand has one carbonyl group that is not involved in the coordination (Fig. 3c). The Th–O (carboxyl) bond lengths are in the range of 2.379(10)–2.578(10) Å and the Th–O (water) bond length is 2.485(12) Å. Both the metal cation and the ligand are 6-fold node (Fig. 3d).

3.2 Specific surface area and porosity

N_2 sorption measurements were performed to evaluate the porous nature of the three kinds of compounds. The N_2 sorption measurements were investigated by the reversible N_2 adsorption and desorption isotherm at 77 K which were shown in typical type-I adsorption isotherms. Compound **1**, **2**, and **3** exhibit a specific BET surface area of 342 $m^2\ g^{-1}$, 408 $m^2\ g^{-1}$, and 283 $m^2\ g^{-1}$, respectively (Fig. S3†). The data is smaller than those of Th-NU-905, Th-NU-1008 and Th-NU-1011 synthesized by the same tetradentate ligand, which are approximately 700–800 $m^2\ g^{-1}$.[11,21] The micropore volume of compound 1, 2, and 3

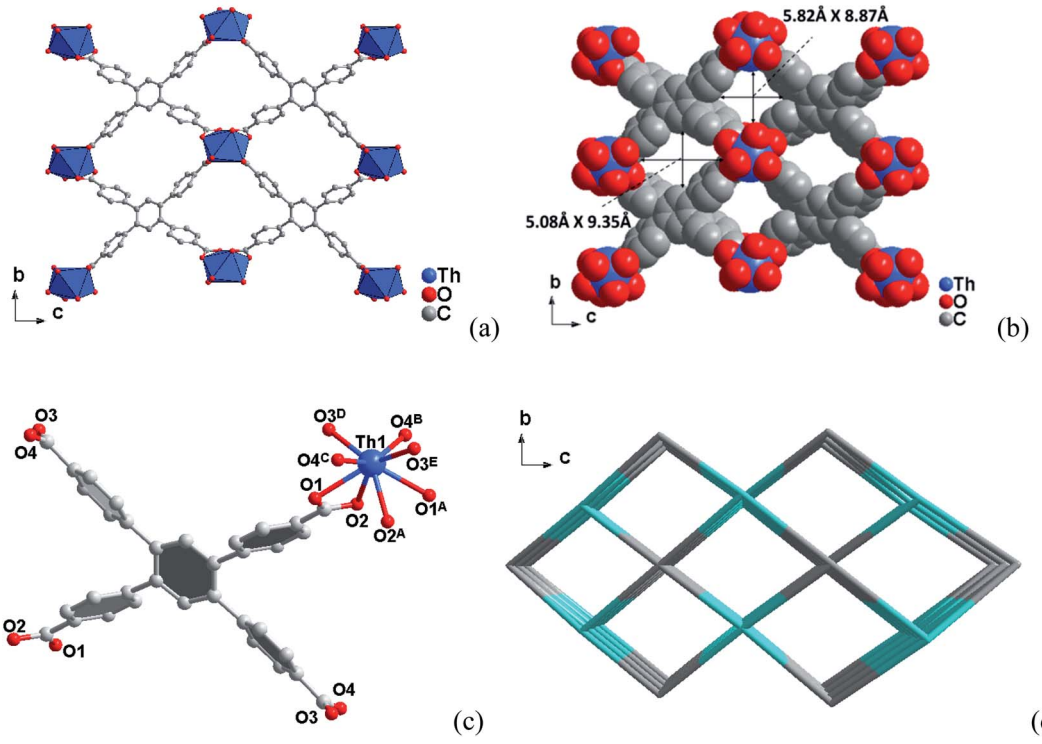

Fig. 1 (a) Three-dimensional framework structure of compound **1** along the *a* axis. (b) The corresponding space-filling models with the pore diameters obtained by taking the van der Waals radii. (c) Coordination environments of the Th(IV) sites in compound **1**. (d) Topology framework for compound **1** showing the channels along [100] direction.

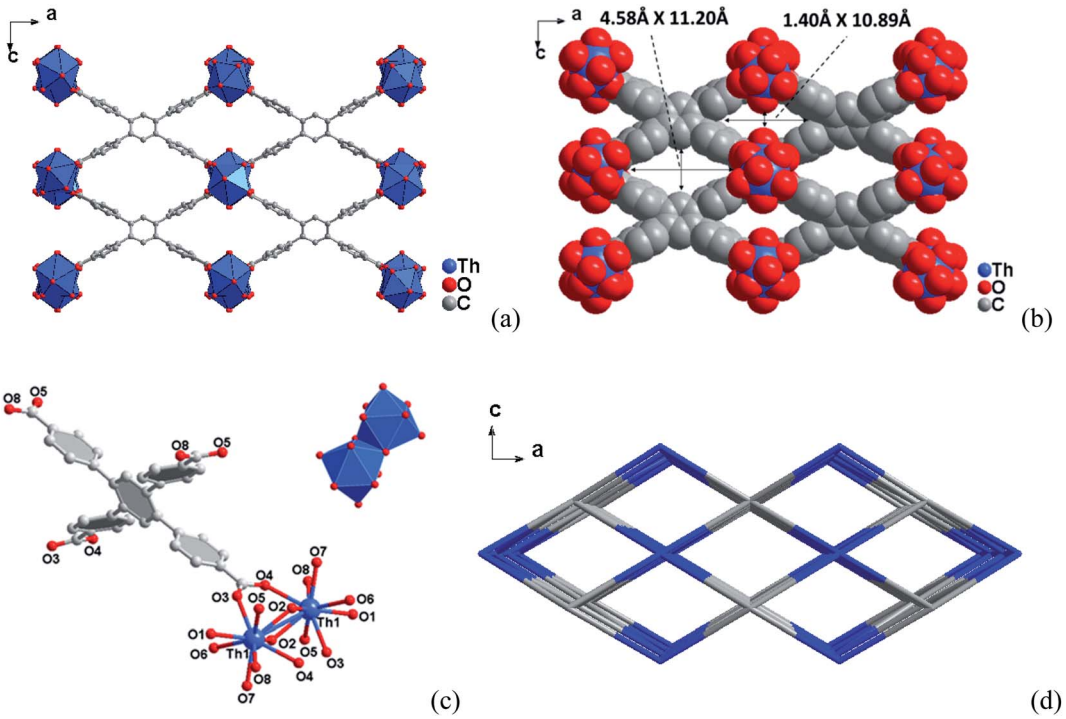

Fig. 2 (a) View along the *b* axis of the structure of compound **2**. (b) The corresponding space-filling models with the pore diameters obtained by taking the van der Waals radii. (c) Coordination environments of the Th(IV) sites in compound **2** and dimer of $Th_2O_3(H_2O)_4(CO_2)_2(CO)_4$. (d) Topology framework for compound **2** showing the channels along [010] direction.

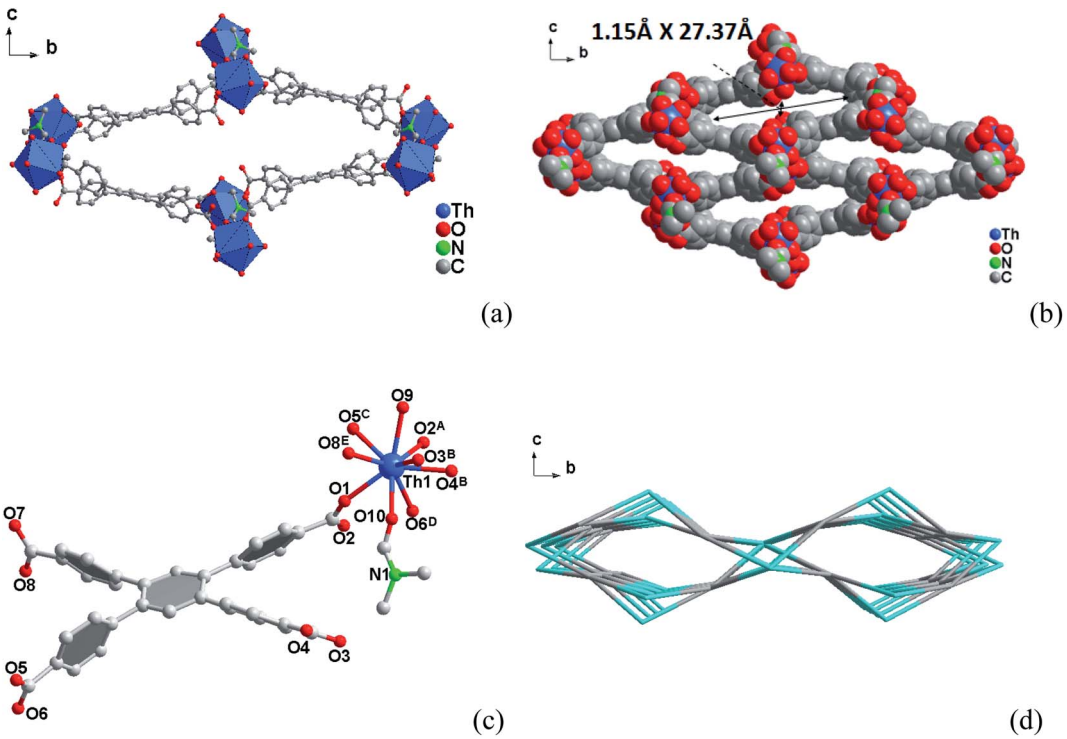

Fig. 3 A view of the three-dimensional framework structure of compound **3** in the [*bc*] plane. (b) The corresponding space-filling models with the pore diameters obtained by taking the van der Waals radii. (c) Coordination environments of the Th(IV) sites in compound **3**. (d) Topology framework for compound **3** showing the channels along [100] direction.

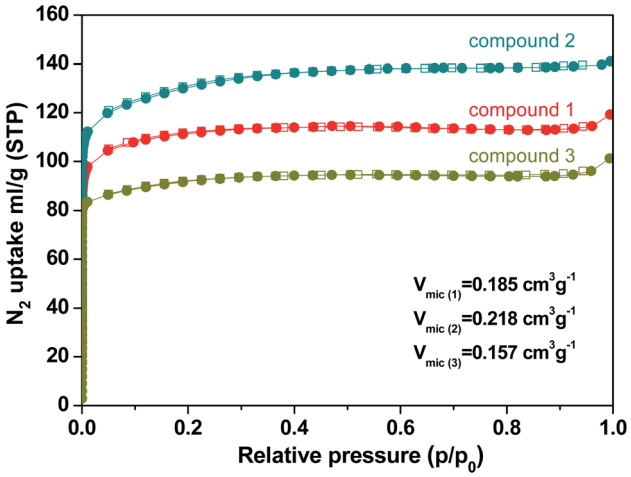

Fig. 4 N_2 adsorption/desorption isotherms of compound **1**, **2**, and **3**.

were 0.185 cm^3 g^{-1}, 0.218 cm^3 g^{-1}, and 0.157 cm^3 g^{-1}, respectively (Fig. 4). The micropore volume order of the three compounds is consistent with the space occupied by solvent and water molecules in the crystal obtained by thermogravimetric calculation. Moreover, the pore size distribution of compound 1, 2, and 3 was 5–12 Å, 5–15 Å, and 7–26 Å, respectively (Fig. S4†).

3.3 Thermal properties

TGA diagram of compound **1**, **2**, **3** in nitrogen atmosphere is shown in Fig. S5.† Each compound loses water molecules, solvent molecules, and coordination water in the pores before 350 °C. Compound **1** weightlessness 24.59%; compound **2** weightlessness 37.92%; compound **3** weightlessness 17.08%. The structural collapse temperatures of compound **1**, **2**, and **3** were 573.66 °C, 532.48 °C, and 582.29 °C, respectively. TGA results show that the prepared MOFs structure can maintain high temperature, which is comparable with the most thermally stable thorium(IV)-based MOFs.[31]

3.4 Irradiation stability

Compound **1**, **2**, and **3** had good γ irradiation stability (Fig. S6†). After a total dose of 20–100 kGy γ irradiation for 7 hours, the PXRD patterns of each crystal after irradiation showed that its frame structure still existed and did not collapse within the radiation intensity determined by the experiment. All these materials had radiation resistance comparable to that of SCU-14,[32] a uranium-based MOF which was irradiated continuously at a cumulative dose of 120 kGy with little change in photoelectric response.

3.5 Luminescence properties

Under visible light, compound **1** and compound **3** are colorless, while compound **2** is pale yellow. All three crystals emit bluish light when exposed to ultraviolet light at 365 nm (Fig. 5). When the excitation is at 360 nm, the emission spectra of compound **1** (Fig. S8a†) and compound **3** (Fig. S8c†) shows broad emission bands with a maximum at 420 nm. However, the emission spectrum of compound **2** consists of a broad band with a maximum at 392 nm (λ_{ex} = 350 nm, Fig. S8b†). The luminescence spectra of all the three thorium-based MOFs are similar to the ligand H4TCPB.[27] This is the same with Zr-CAU-24, which indicates that the luminescence is mostly attributed to the emission of the organic linker. Some differences still exist. The intensity of the emission spectra of compound **1** and compound **3** increased and redshifted slightly, while compound **2** has a slightly blue shifted emission spectrum with reduced intensity. Compound **2** is the central unit of a dinuclear cluster, which is distinct from the mononuclear unit of compound **1** and compound **3**. The variation of thorium coordination environment may be the cause of the above differences. Although thorium is a non-luminescence metal center, different nuclear clusters change the bond length and bond angle of Th–O–C, and then affect the electron density of the bonded benzene rings in the ligand, resulting in a slight change in the excitation spectrum.

4. Conclusion

In summary, three new thorium-based MOFs were synthesized in H4TCPB, DMF, and trifluoroacetic acid reactive systems. Compound **1** and compound **3** are the mononuclear MOFs of the monoclinal system, while compound **2** is the binuclear cluster MOF of the orthorhombic system. The thermal stability of the synthetic thorium-based MOFs is higher than 500 °C and exhibits good γ irradiation stability. N_2 sorption experiments reveal the specific BET surface area of 342 m^2 g^{-1}, 408 m^2 g^{-1},

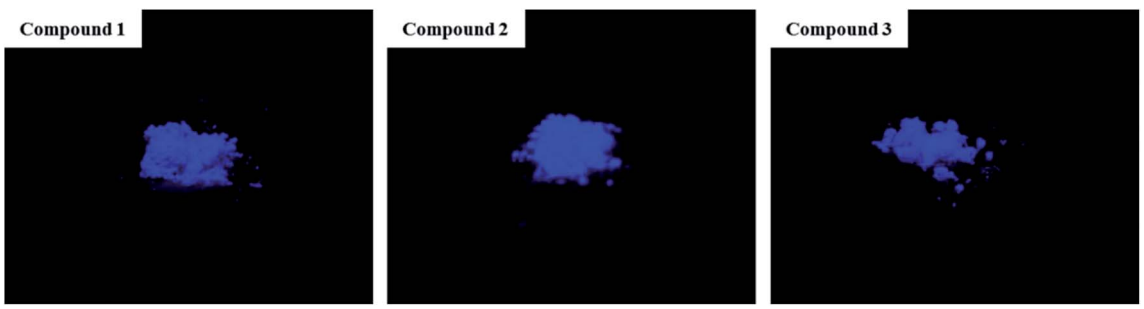

Fig. 5 Images of compound **1**, **2**, and **3** at UV wavelength 365 nm.

283 $m^2 g^{-1}$ and the micropore volume of 0.185 $cm^3 g^{-1}$, 0.218 $cm^3 g^{-1}$, 0.157 $cm^3 g^{-1}$ for compound **1**, **2**, and **3**, respectively. All the complexes emit blue ligand-based luminescence, while the emission spectrum of compound **2** is slightly blue-shifted and reduced in intensity compared with the others.

Conflicts of interest

There are no conflicts to declare.

Acknowledgements

Supported by Spent nuclear fuel reprocessing special project: computer simulation and software development of reductive stripping of Plutonium(1B, 2B) in PUREX(BG17000303). The authors thank the "Young Potential Program of Shanghai Institute of Applied Physics, Chinese Academy of Sciences" (Y955031031) for the equipment applied in this work.

References

1 U. Mueller, M. Schubert, F. Teich, P. K. Schierle-Arndt, J. Pastre and J. Mater, *Chem*, 2006, **16**(7), 626–636.
2 J. Li, X. X. Wang, G. X. Zhao, C. L. Chen, Z. F. Chai, A. Alsaedi, T. Hayatf and X. K. Wang, *Chem. Soc. Rev.*, 2018, **47**, 2322–2356.
3 E. A. Dolgopolova, A. M Rice and N. B. Shustova, *Chem. Commun.*, 2018, **54**, 6472.
4 S. L. Hanna, X. Zhang, K. I. Otake, R. J. Drout, P. Li, T. Islamoglu and O. K. Farha, *Cryst. Growth Des.*, 2019, **19**(1), 506–512.
5 P. M. Cantos and C. L. Cahill, *Cryst. Growth Des.*, 2014, **14**, 3044–3053.
6 Z. H. Zhang, G. A. Senchyk, Y. Liu, T. Spano-Franco, J. E. S. Szymanowski and P. C. Burns, *Inorg. Chem.*, 2017, **56**, 13249–13256.
7 P. Thuéry, E. Rivière and J. Harrowfield, *Inorg. Chem.*, 2015, **54**, 2838–2850.
8 M. B. Andrews and C. L. Cahill, *Angew. Chem., Int. Ed.*, 2012, **51**, 6631–6634.
9 L. Shao, F. W. Zhai, Y. L. Wang, G. Z. Yue, Y. R. Li, M. F. Chu and S. Wang, *Dalton Trans.*, 2019, **48**, 1595–1598.
10 C. Ekberg, Y. Albinsson, M. J. Comarmond and P. L. Brown, *J. Solution Chem.*, 2000, **29**, 63–86.
11 P. Li, X. J. Wang, K. Otake, J. F. Lyu, S. L. Hanna, T. Islamoglu and O. K. Farha, *ACS Appl. Nano Mater.*, 2019, **2**(4), 2260–2265.
12 J. Y. Kim, A. J. Norquist and D. O'Hare, *J. Am. Chem. Soc.*, 2003, **125**(42), 12688–12689.
13 K. M. Ok, J. Sung, G. Hu, R. M. Jacobs and D. O'Hare, *J. Am. Chem. Soc.*, 2008, **130**(12), 3762–3763.
14 K. M. Ok and D. O'Hare, *Dalton Trans.*, 2008, (No. 41), 5560–5562.
15 N. P. Martin, C. Volkringer, C. M. Falaise, N. Henry and T. Loiseau, *Cryst. Growth Des.*, 2016, **16**(3), 1667–1678.
16 Y. Wang, W. Liu, Z. Bai, T. Zheng, M. A. Silver, Y. Li, Y. Wang, X. Wang, J. Diwu, Z. Chai and S. Wang, *Angew. Chem.*, 2018, **130**(20), 5885–5889.
17 Y. Li, Z. Yang, Y. Wang, Z. Bai, T. Zheng, X. Dai, S. Liu, D. Gui, W. Liu, M. Chen, L. Chen, J. Diwu, L. Zhu, R. Zhou, Z. Chai, T. E. Albrecht-Schmitt and S. Wang, *Nat. Commun.*, 2017, **8**(1), 1354.
18 G. Sargazi, D. Afzali and A. Mostafavi, *Ultrason. Sonochem.*, 2018, **41**, 234–251.
19 J. Andreo, E. Priola, G. Alberto, P. Benzi, D. Marabello, D. M. Proserpio, C. Lamberti and E. Diana, *J. Am. Chem. Soc.*, 2018, **140**(43), 14144–14149.
20 C. M. Falaise, J. S. B. Charles, C. Volkringer and T. Loiseau, *Inorg. Chem.*, 2015, **54**(5), 2235–2242.
21 P. Li, S. Goswami, K. Otake, X. J. Wang, Z. J. Chen, S. L. Hanna and O. K. Farha, *Inorg. Chem.*, 2019, **58**, 3586–3590.
22 T. Islamoglu, D. Ray, P. Li, M. B. Majewski, I. Akpinar, X. Zhang, C. J. Cramer, L. Gagliardi and O. K. Farha, *Inorg. Chem.*, 2018, **57**(21), 13246–13251.
23 Z. J. Li, Y. Ju, B. W. Yu, X. L. Wu, H. J. Lu, Y. X. Li, J. Zhou, X. F. Guo, Z. H. Zhang, J. Lin, J. Q. Wang and S. Wang, *Chem. Commun.*, 2020, **56**, 6715–6718.
24 Z. J. Li, Z. H. Yue, Y. Ju, X. L. Wu, Y. M. Ren, S. F. Wang, Y. X. Li, Z. H. Zhang, X. F. Guo, J. Lin and J. Q. Wang, *Inorg. Chem.*, 2020, **59**, 4435–4442.
25 G. E. Gomez, J. A. Ridenour, N. M. Byrne, A. P. Shevchenko and C. L. Cahill, *Inorg. Chem.*, 2019, **58**(11), 7243–7254.
26 S. Saumitra and B. Udo, *RSC Adv.*, 2015, **5**, 26735–26748.
27 M. Lammert, H. Reinsch, C. A. Murray, M. T. Wharmby, H. Terraschkea and N. Stock, *Dalton Trans.*, 2016, **45**, 18822–18826.
28 O. V. Dolomanov, L. J. Bourhis, R. J. Gildea, J. A. K. Howard and H. Puschmann, *J. Appl. Crystallogr.*, 2009, **42**, 339–341.
29 G. M. Sheldrick, *Acta Crystallogr., Sect. A: Found. Adv.*, 2015, **A71**, 3–8.
30 G. M. Sheldrick, *Acta Crystallogr., Sect. C: Struct. Chem.*, 2015, **C71**, 3–8.
31 K. P. Carter, J. A. Ridenour, M. Kalaj and C. L. Cahill, *Chem.–Eur. J.*, 2019, **25**, 7114–7118.
32 L. W. Cheng, C. Y. Liang, W. Liu, Y. X. Wang, B. Chen, H. L. Zhang, Y. L. Wang, Z. F. Chai and S. Wang, *J. Am. Chem. Soc.*, 2020, **142**(38), 16218–16222.